

Geophysical Research Letters[®]



RESEARCH LETTER

10.1029/2021GL094552

Key Points:

- Pore pressure imaging of Mt. Pollino evidences that seismic sequence occurred in a fluid-filled volume at pressure higher than hydrostatic
- Pore pressure diffusion analysis suggests that seismicity distribution was driven by relatively low diffusivity value

Supporting Information:

Supporting Information may be found in the online version of this article.

Correspondence to:

R. De Matteis,
raffaella.dematteis@unisannio.it




Citation:

De Matteis, R., Convertito, V., Napolitano, F., Amoroso, O., Terakawa, T., & Capuano, P. (2021). Pore fluid pressure imaging of the Mt. Pollino region (southern Italy) from earthquake focal mechanisms. *Geophysical Research Letters*, 48, e2021GL094552. <https://doi.org/10.1029/2021GL094552>

Received 10 JUN 2021

Accepted 8 NOV 2021

Pore Fluid Pressure Imaging of the Mt. Pollino Region (Southern Italy) From Earthquake Focal Mechanisms

R. De Matteis¹ , V. Convertito² , F. Napolitano³ , O. Amoroso³ , T. Terakawa⁴ , and P. Capuano³ 

¹Dipartimento di Scienze e Tecnologie, Università degli Studi del Sannio, Benevento, Italy, ²Istituto Nazionale di Geofisica e Vulcanologia, Osservatorio Vesuviano, Napoli, Italy, ³Dipartimento di Fisica "E.R.Caianello", Università degli Studi di Salerno, Fisciano, Italy, ⁴Earthquake and Volcano Research Center, Graduate School of Environmental Studies, Nagoya University, Nagoya, Japan

Abstract Focal mechanisms of selected earthquakes, recorded in the Mount Pollino region (southern Italy) from 2010 through 2014, are used to infer the pore fluid pressure at hypocenter depths. The 3-D excess pore pressure field provides evidence that the sequence occurs in a fluid-filled volume with values reaching 35 MPa. The mechanisms underlying this swarm-like sequence and the triggering of earthquakes are investigated by computing the cumulative static Coulomb stress change at hypocenter depths and analyzing the pore-pressure diffusion mechanism. The results indicate that static Coulomb stress change was lower than 0.01 MPa, which is the value generally assumed as threshold for the triggering, and seismicity distribution was actually driven by pore-pressure diffusion with relatively low diffusivity value. This latter mechanism could also explain the delayed triggering of the two larger events M_L 4.3 and M_L 5.0, respectively, that occurred about 150 days apart.

Plain Language Summary Between 2010 and 2014, a seismic sequence of about 10,000 small-to-moderate earthquakes was recorded in the Mount Pollino region, one of the most seismic hazardous areas of Italy. The physical mechanism underlying the swarm-like sequence is not yet adequately understood, and in this study, the role of fluids is investigated. The 3D distribution of the pore fluid pressure, obtained from focal mechanisms, evidences that the sequence occurred in a fluid-filled volume at pressure higher than hydrostatic value, and explains the triggering of events also on faults non-optimally oriented with respect to the regional stress pattern. Furthermore, the timing of the sequence evolution is studied by exploiting the contribution of Coulomb static stress change and the role of pore-pressure diffusion mechanism.

1. Introduction

The Mount Pollino region, located at the transitional area between the end of the southern Apennines and the northern part of the Calabrian arc (southern Italy), has been identified as one of the most hazardous seismic gaps in the intra-Apennine seismogenic belt of Italy (Cinti et al., 1997; Valensise & Guidoboni, 2000). The analysis of seismological data (Frepoli et al., 2011; Maggi et al., 2009; Napolitano et al., 2021; Totaro et al., 2013, 2015) and geodetic measurements (Ferranti et al., 2014; Palano et al., 2017; Serpelloni et al., 2005) suggest a dominant northeast-southwest extensional regime in the central part of the Pollino range that results in an intricate system of faults. The revision of some historical earthquakes, such as the 1693 (M_w 5.3) and 1708 (M_w 5.6) earthquakes (Camassi et al., 2011; Tertulliani & Cucci, 2014), indicated that these events occurred during long sequences, suggesting that repeating swarm-like sequences could characterize the seismicity of the Pollino region, at least during the last 400 years (Passarelli et al., 2015). The most recent earthquake occurred on September 9, 1998, with a magnitude M_w 5.6 activating the CSPT fault (Figure 1) (Brozzetti et al., 2009; Michetti et al., 2000).

Between 2010 and 2014, a sequence of small-to-moderate earthquakes occurred just west of Mt. Pollino, located at 4–15 km depth (Passarelli et al., 2015; Totaro et al., 2013) (Figure 1). The sequence was characterized by about 10,000 earthquakes with local magnitude ranging between 0.5 and 5.0, with two strongest events M_L 4.3 and M_L 5.0 occurred on May 28, 2012 in the eastern sector and on October 25, 2012 in the western sector. The architecture and kinematics of the seismogenic faults of the area have been previously studied

© 2021. The Authors.

This is an open access article under the terms of the [Creative Commons Attribution-NonCommercial-NoDerivs](https://creativecommons.org/licenses/by/4.0/) License, which permits use and distribution in any medium, provided the original work is properly cited, the use is non-commercial and no modifications or adaptations are made.

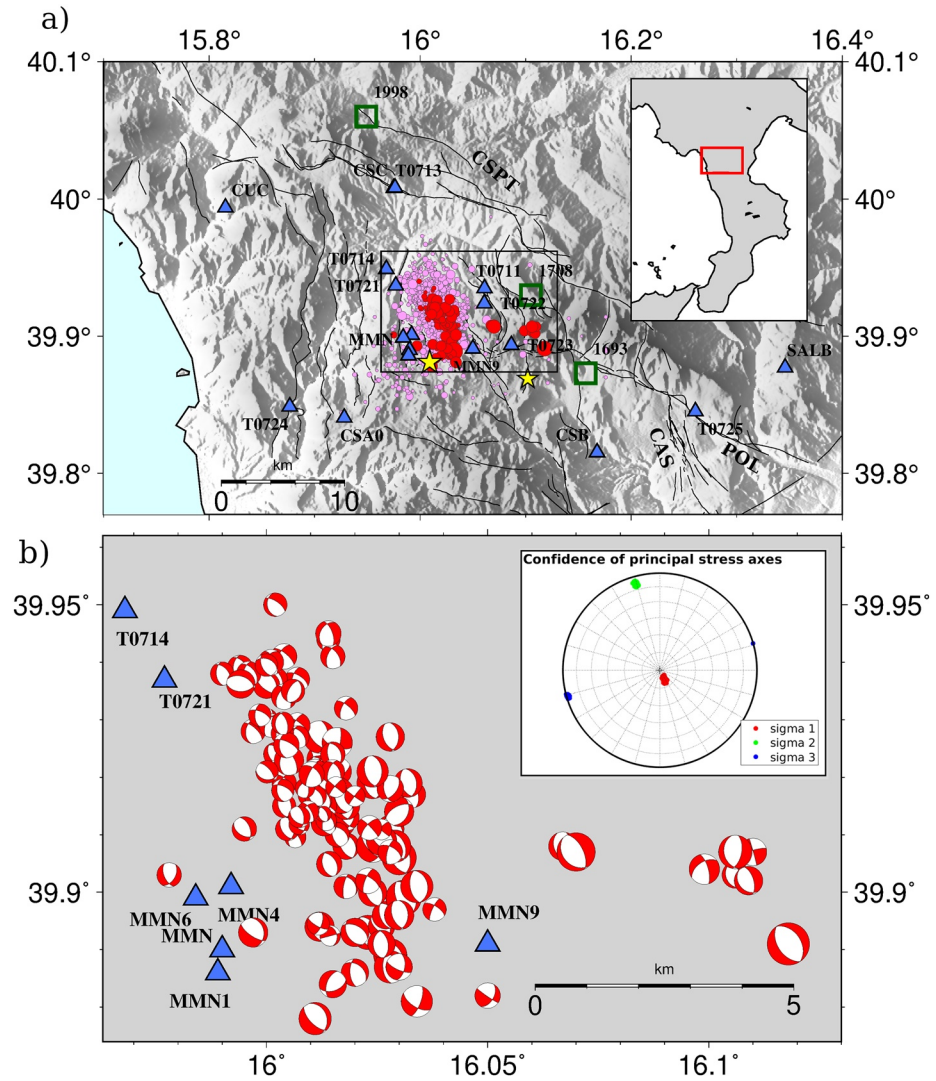


Figure 1. (a) The 2010–2014 Mt. Pollino sequence (pink circles). Blue triangles represent the seismic stations and red circles are the earthquake epicenters for which focal mechanisms are available. Size of symbol scales with magnitude. The map shows the epicenters of both some historical earthquakes (green squares) and the two largest events M_L 4.3 and M_L 5.0 (yellow stars). The black rectangle indicates the area shown in the lower panel. Black lines represent the faults including CSPT (Castelluccio and Castello Seluci-Piana Perretti-Timpa della Manca Faults), POL (Pollino Fault), and CAS (Castrovillari Faults). (b) Map of the 120 focal mechanisms. The size of beachball scales with magnitude. The inset shows the stereographic projection of the principal stress axes obtained by Napolitano et al. (2021).

by Totaro et al. (2015), that computed high precision locations and focal mechanisms of events $M_L > 2.6$. Clusters of events of extremely similar waveforms have been then relocated by Napolitano et al. (2021) and new focal mechanisms of events ($1.0 < M_L < 2.8$) have been provided.

The physical mechanism underlying the long-lasting swarm-like sequence is not yet adequately understood, although several mechanisms such as Coulomb stress change, dynamic triggering, aseismic processes, and pore pressure perturbation (Convertito et al., 2020 and references therein) are invoked. The space and time evolution of the seismic sequences occurring in the last two decades in Italy (e.g., the 1997 Colfiorito sequence (Miller et al., 2004), the 2009 L'Aquila earthquake (Di Luccio et al., 2010; Malagnini et al., 2012), the 2016 Amatrice sequence (Convertito et al., 2020; Tung & Masterlark, 2018)), have been ascribed to the effect of fluid flow and/or pore pressure diffusion. Similar to the above-mentioned sequences, the Pollino sequence occurred in an extensive tectonic regime. Some authors have suggested a relation between the fluid flow and the tectonic regime (e.g., Dogliani et al., 2014; Miller, 2020; Muir-Wood & King, 1993). In

particular, Valerio et al. (2017) found a relationship between the aftershock duration and tectonic regime with longer duration in extensional regimes due to a joint effect of gravitational forces and pure elastic stress release. Miller (2020) has proposed a correlation between aftershock decay rates and the tectonic ability to heal the co-seismically and post-seismically generated fracture networks. According to this model, rich and long-lasting aftershock sequences are expected in areas characterized by extensional regimes due to their little ability to close fractures for propagating deeply trapped fluids.

Passarelli et al. (2015) found that the spatial and temporal behavior of the Pollino sequence is consistent with the general characteristics of swarm-like seismicity. In particular, they concluded that only 25% of the earthquakes follows the Omori law, and attributed the leftover 75% to additional physical processes such as fluid infiltration at crustal depth, pore pressure diffusion, or transient and aseismic slip episodes. Later, Cheloni et al. (2017), using geodetic (GPS and DInSAR) and seismological observations, provided the evidence that a transient aseismic slip event may be the main driver of the whole seismic sequence.

The presence of fluids has also been suggested by Napolitano et al. (2020), who used the Pollino sequence to map scattering and absorption in the area. The results are confirmed by Sketsiou et al. (2020). Moreover, the 3-D attenuation image obtained by Sketsiou et al. (2021), using the coda normalization method, provides evidence of the presence of fluid storage. As a further evidence of the presence of a highly fractured fluid-filled volume, Barberi et al. (2004), Piana Agostinetti and Amato (2009), and Totaro et al. (2014) have found pronounced anomaly of high v_p / v_s ratio (>1.9) at 0–10 km depth.

The goal of the present study is to investigate the role of fluids during the sequence. To this aim, we apply the focal mechanism tomography (FMT) technique developed by Terakawa et al. (2010), to focal mechanisms of the Mt. Pollino sequence, to image the 3D time-independent distribution of the excess pore fluid pressure above hydrostatic pressure. We also discuss the timing of the sequence evolution by exploiting the contribution of Coulomb static stress change and the role of a homogeneous isotropic diffusivity mechanism.

2. Focal Mechanism Tomography

We apply the FMT technique proposed by Terakawa et al. (2010) to estimate the 3D excess pore fluid pressure field at earthquakes depth. Under a known regional stress field, FMT assumes a constant friction coefficient and attributes the focal mechanism variations to fault strength heterogeneity due to different pore fluid pressure acting on faults. Three main hypotheses must be verified for FMT to be effective: (a) the fault strength is controlled by Coulomb failure criterion:

$$\tau = \mu(\sigma_n - P) \quad (1)$$

where τ and σ_n are the shear and normal stress on the fault plane, respectively, P is the pore fluid pressure, and μ is the friction coefficient, assumed constant; (b) the slip vector is parallel to the direction of the shear stress acting on the fault plane (Bott, 1959; Wallace, 1951); (c) the failure occurs on optimally oriented fault relative to the regional stress field under hydrostatic pressure (see Supporting Information S1 for details). Thus, to evaluate the 3D pore fluid pressure through FMT, we must estimate the stress field acting in the study area. Several inverse methods have been developed for finding the stress field orientation using fault plane solutions. The most standard one is a method to estimate the stress pattern from slip vectors of events, based on the hypothesis that the tangential traction on the fault plane should be parallel to the slip direction (e.g., Michael, 1987). The stress tensor that best fits the data is represented by the orientation of the three principal stress axes, and the scalar R (stress ratio), which describes the relative magnitudes of the principal stresses and hence constrains the shape of the deviatoric stress ellipsoid. With regard to the magnitude of the principal stresses, we use hypotheses (a) and (c) and the assumption that vertical stress is the weight of the overburden. Then, we can calculate the normal and shear stresses on the two nodal planes of focal mechanisms, and the fault plane is identified as the nodal plane for which the value of the angle between the slip vector and the shear stress direction is smaller. Finally, the pore fluid pressure is evaluated by using the Coulomb failure criterion (Equation 1). From discrete fluid pressure at the hypocenters, we estimated the 3D pore fluid pressure field and associated uncertainty (Terakawa et al., 2010, 2012). The technique applies an inversion scheme developed by Yabuki and Matsu'ura (1992), based on the Bayesian statistical inference and Akaike's Bayesian Information Criterion.

3. Data and Analysis

During the seismic crisis the permanent national seismic network, managed by Istituto Nazionale di Geofisica e Vulcanologia (INGV), was improved by the installation of temporary seismic networks in the epicentral area by the Università della Calabria (since October 2010) and INGV (since November 2011) (Margheriti et al., 2013; Totaro et al., 2016). The enhanced number of stations allowed estimating high-quality focal mechanisms even for earthquakes as small as M_L 1.0 (Napolitano et al., 2021; Totaro et al., 2013, 2015).

The data set consists of the well-constrained focal mechanisms of 120 earthquakes of the seismic sequence occurring between 2010 and 2014 in the Pollino Mountains area (Figure 1). We used 47 focal mechanisms computed by Totaro et al. (2015) and 73 focal mechanisms provided by Napolitano et al. (2021). The focal mechanisms are highly homogeneous: the majority of fault plane solutions show a dominant normal-faulting mechanism with pure normal fault and normal fault with a strike-slip component, and only a few solutions show strike-slip kinematics for shallowest events (Figure 1b). The solutions are consistent with the principal trend of the faults in the area and the extensional stress field characterized by a nearly horizontal minimum compressive stress axis, perpendicular to fault orientation (Brozzetti et al., 2017; Ferranti et al., 2017; Totaro et al., 2016).

Although the Pollino sequence lasted about 4 years, most of the events, for which focal mechanisms are available, occurred at the end of 2011 and in 2012, in particular in October and November. Thus, the data set only allows estimating a static image of pore pressure field.

We used the stress pattern estimated by Napolitano et al. (2021) from the inversion of the 120 focal mechanisms. The results (Figure 1b) show a stress pattern characterized by stress ratio $R = (\sigma_1 - \sigma_2)/(\sigma_1 - \sigma_3)$ equal to 0.35, a nearly vertical maximum compressive principal axis σ_1 (trend 149° , plunge 82°) and a nearly horizontal minimum compressive principal axis σ_3 (trend 75° , plunge 2°), revealing the existence of a dominant NE-SW extensional regime in good agreement with the results obtained from the analysis of other structural, seismological and geophysical data. We note that Napolitano et al. (2021) used the iterative method by Vavrycuk (2014) that jointly inverts for stress and fault orientations, selecting the fault plane between the two nodal planes. However, in the following FMT analysis, we estimate the excess pore fluid pressure on both nodal planes of the focal mechanisms.

To estimate the magnitude of the principal stresses, we start from the calculation of the lithostatic pressure $\sigma_v = \rho gz$, where σ_v is the vertical stress, z the depth, ρ the density, and g is the gravity acceleration. At each depth, the density value is calculated by using the empirical relation between the P-wave velocity and density proposed by Brocher (2005):

$$\rho(g / cm^3) = 1.6612V_p - 0.4721V_p^2 + 0.0671V_p^3 - 0.0043V_p^4 + 0.000106V_p^5 \quad (2)$$

where the P-wave velocity in km/s at each depth has been obtained from the 1D model proposed by Barberi et al. (2004). Then, bearing in mind that the depth of the hypocenters varies between 4 and 10 km, the average density value of $2,510 \text{ kg/m}^3$ was calculated. Next, to estimate the intensity of σ_1 , σ_2 and σ_3 as function of depth, we use the constraint on σ_v and the hypothesis (c), that is, the following relation (Zoback, 2010):

$$\frac{\sigma_1 - P}{\sigma_3 - P} = \left[(\mu^2 + 1)^{1/2} + \mu \right]^2 \quad (3)$$

The knowledge of the stress field allows us to calculate the normal and shear stress acting on the two nodal planes of the selected focal mechanisms. We choose as the fault plane the nodal plane with the smaller angle (misfit angle) between the actual slip vector and the resolved shear stress acting on the same plane. If the two misfit angles differ by less than 10° , we select as fault plane the nodal plane with lower fluid pore pressure.

In the subsequent analysis, we consider only the events for which the misfit angle is smaller than 15° , obtaining a data set of 86 earthquakes (with average misfit angle equal to 7° and standard deviation equal to 4°) for which the pore fluid pressure is calculated by using Equation 1.

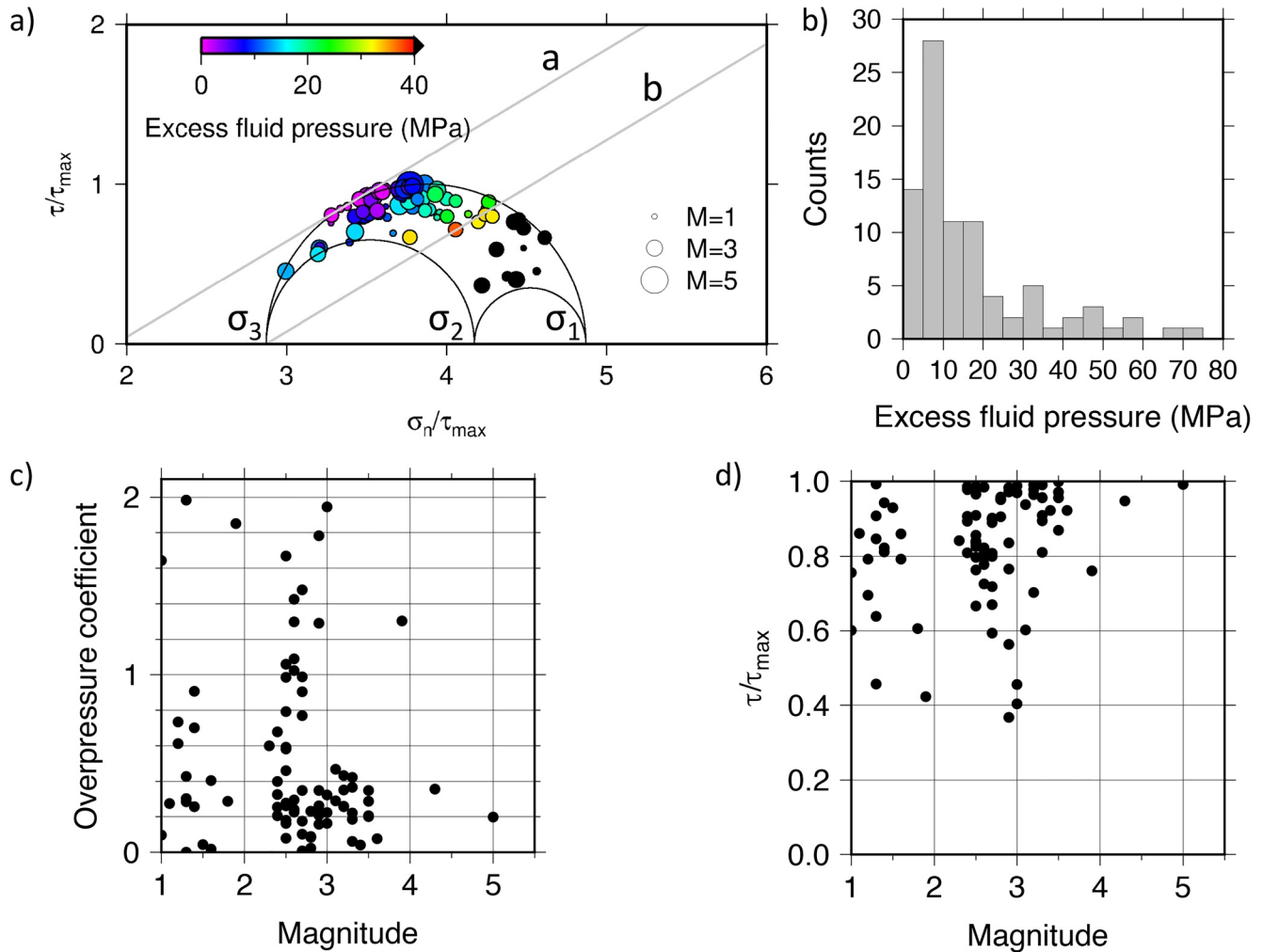


Figure 2. (a) Mohr diagram normalized by the maximum shear stress. The circles represent the normalized normal and shear stress acting on the fault plane for the 86 earthquakes, the color indicates the excess fluid pressure, and the size scales with magnitude. The gray lines *a* and *b* indicate fault strength under hydrostatic and lithostatic fluid pressures, respectively. (b) Histogram of excess fluid pressures. (c, d) Overpressure coefficient and shear stress normalized by maximum shear stress as function of magnitude.

The shear and normal stress acting on a plane within a uniform stress pattern can be represented by a point on the 3D Mohr diagram, in the region delimited by the three Mohr circles (Figure 2a). According to hypothesis (c), if the slip plane is optimally oriented relative to the stress field pattern, the point lies on the great circle where the Mohr-Coulomb failure line under hydrostatic pressure is tangent to Mohr's circle. For an unfavorably oriented plane, an excess of pore fluid pressure with respect to hydrostatic pressure provokes failure.

Figure 2b shows the distribution of the excess pore fluid pressure highlighting that most of the earthquakes occurred at values between 1 and 30 MPa, in particular the two strongest events M_L 4.3 and M_L 5.0 occurred at about 8 and 12 MPa, respectively. To obtain estimation independent from the depth, we compute the excess of pore pressure normalized by the difference between minimum principal stress σ_3 and hydrostatic pressure (overpressure coefficient, Terakawa et al., 2012) and the shear stress normalized by the maximum shear stress value. Interestingly, the overpressure coefficient as a function of events' magnitude suggests that most of the earthquakes (including the largest ones) are triggered by pore fluid pressure higher than hydrostatic value (Figure 2c) on faults unfavorably oriented (Figure 2d). Few events have overpressure coefficient about zero—indicating that they occurred on favorably oriented faults—or are characterized by

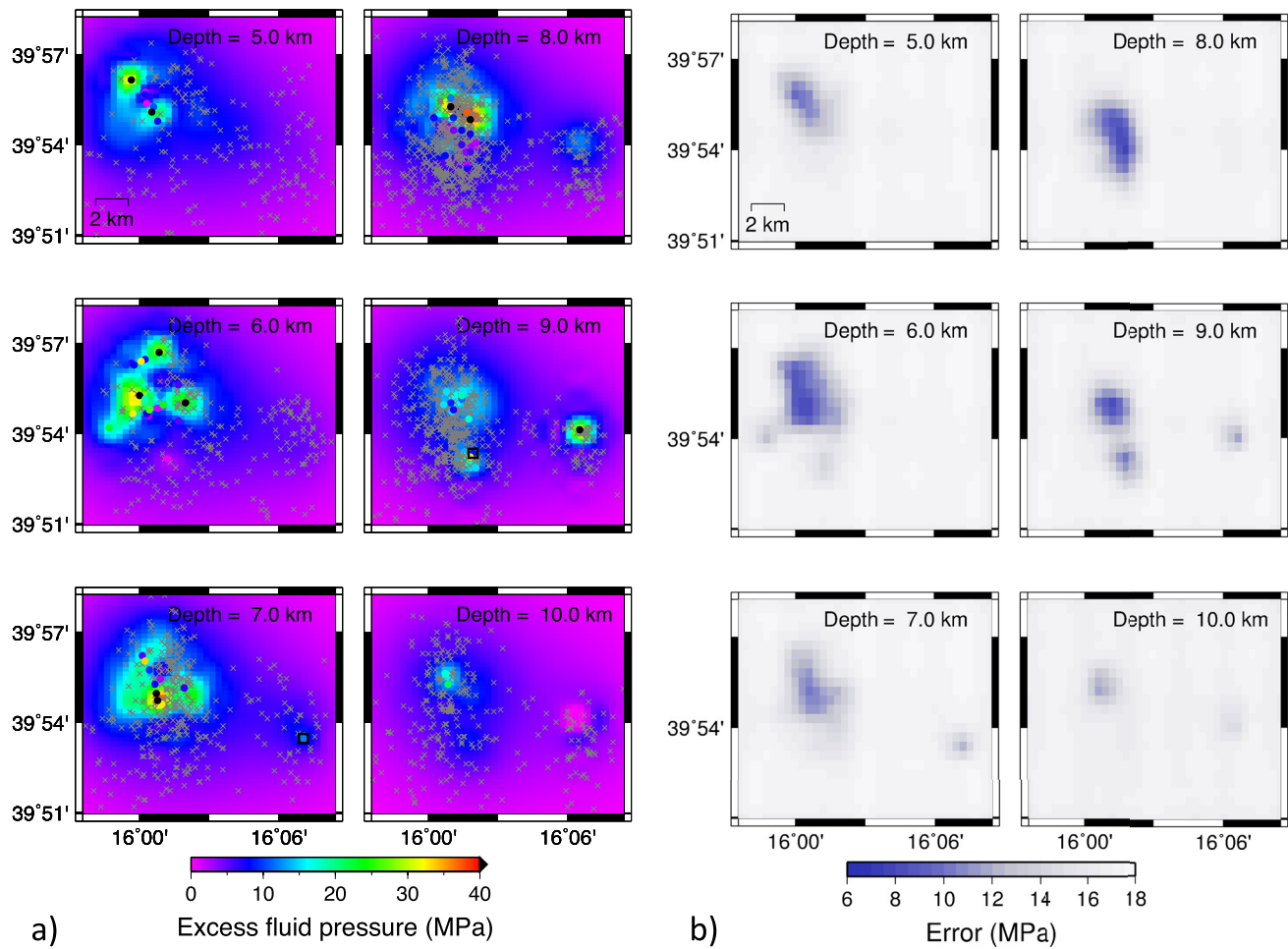


Figure 3. (a) Maps of the excess pore fluid pressure field at different depths, and associated standard deviation in panel (b). The circles represent, in a range of 1 km around each layer, the location of the 86 earthquakes used to estimate the fluid pressure distribution. Black squares represent the location of the two largest events. All events of the seismic sequence with $M > 1.3$ are also superimposed on the maps (gray crosses).

pore fluid pressure greater than σ_3 , likely due to a non-double couple component in the focal mechanism or local stress heterogeneity.

4. Excess Pore Fluid Pressure Imaging

The previous analysis, through Equation 1, allowed estimating the values of the excess pore pressure at the hypocenter of the 86 selected earthquakes. In order to obtain the 3D pore fluid pressure field as a continuous function and associated uncertainty, we apply the technique developed by Terakawa et al. (2010, 2012) to these discrete fluid pressure measurements (see Supporting Information S1 for details). The dimensions of the investigated volume around the sequence are $16 \times 14 \times 10 \text{ km}^3$ (along East, North, and vertical, respectively) and we distribute 4,199 ($19 \times 17 \times 13$) tri-cubic B-splines with 1 km equally spaced local support (grid interval), which represents a measure of spatial resolution. The results of the inversion technique are represented as map view, at different depths, of the excess pressure and the standard error. From 5 km up to 9 km depth, a high excess pore pressure region ($\sim 30 \text{ MPa}$) emerges in the volume around the mainshock ($M_L 5.0$). At 9 km depth, an additional limited anomaly is present in the eastward region with an excess pore fluid pressure of $\sim 30 \text{ MPa}$ (Figure 3a). In these overpressure fluid regions, the standard deviation of the excess pore fluid pressure varies between about 6 and 12 MPa (Figure 3b). On the same maps, we also superimpose the hypocenters of the whole sequence. We used the catalog provided by Università della Calabria, and in particular, we show only the events with magnitude above the minimum magnitude of completeness

M_c 1.3, estimated by using the maximum curvature approach (Wiemer & Wyss, 2000). Figure 3a shows that most of the events occurred in a volume with excess pore pressure higher than 5 MPa, providing an evidence of the role played by the fluids during the sequence evolution.

To take into account the uncertainty on the value of friction coefficient, we repeat the previous analysis and estimate the pore fluid pressure field by using μ value equal to 0.4 and 0.8, respectively (Figures S1, S2, S4, and S5 in Supporting Information S1). The differences between the excess pore pressure estimated with $\mu = 0.6$ and these two values are overall less than ~ 7 MPa, and the shape of the high-pressure areas remains unchanged varying the friction coefficient (Figures S3 and S6 in Supporting Information S1). Both for $\mu = 0.4$ and for $\mu = 0.8$, the greatest differences are observed in the lower part of the investigated volume.

5. Discussion and Conclusion

In the present study, we used FMT proposed by Terakawa et al. (2010) to estimate the 3D excess pore fluid pressure in the Mt. Pollino region, and we find that the volume around the seismic sequence is characterized by high excess pore fluid pressure with values reaching ~ 35 MPa and almost all the events ($\sim 4,800$) are located in areas characterized by an excess pore pressure larger than 10–15 MPa (Figure 3a).

It is worth noting that the presence of fluids in this region down to 10 km has been evidenced in previous works based on large scale V_p/V_s anomaly (Barberi et al., 2004; Totaro et al., 2014) and electro-magnetic signals associated with the seismic sequence (Balasco et al., 2014). Furthermore, Napolitano et al. (2020), from the analysis of P-wave scattering and coda-wave attenuation, found that the region investigated in this study is characterized by high scattering/high absorption, and interpreted it as a highly fractured fluid-filled seismogenic volume.

Our results suggest that almost all the events occurred on unfavorably oriented faults requiring pore fluid pressure higher than hydrostatic pressure. Moreover, the role of fluids, in addition to the documented transient aseismic slow slip event (Cheloni et al., 2017), can also be invoked to explain the decay rate of majority of events that Passarelli et al. (2015) found to be different from the rate prescribed by the Omori law.

To further support our findings, we evaluate the contribution of Coulomb static stress change in the seismic sequence evolution. We compute the cumulative static Coulomb stress change due to the 120 earthquakes for which the focal mechanism is available. We use the numerical code developed by Wang et al. (2006) that allows calculating co-seismic and post-seismic deformation in a flat layered crustal model. We adopt the velocity model proposed by Barberi et al. (2004) and use Equation 2 to compute the density at each layer. The friction coefficient μ is set equal to 0.6, while the Skempton coefficient, is set to 0.6. Each event is modeled as planar source whose orientation is given by focal mechanism while the expected dimension and average slip value are obtained by using the Wells and Coppersmith (1994) relationships for normal faults mechanism. Finally, we assume that each receiver fault is optimally oriented with respect to the uniform stress pattern reported in the previous analysis.

Figure 4a shows that while the May 28, 2012, M_L 4.3, event was favored since the beginning of the sequence, the October 25, 2012, M_L 5.0, event was favored only after the occurrence of the previous M_L 4.3 event. Overall, Coulomb stress transfer did not exceed 0.01 MPa, which is considered as a minimum threshold for earthquakes triggering (e.g., King et al., 1994; Reasenberg & Simpson, 1992). However, although it is known that stress change near the source depends on details of slip distribution, dealing with small to light events, the assumption of a uniform slip on the fault may be considered reasonable. It thus remains to explain the delayed triggering of the M_L 5.0 event on October 25. To support the hypothesis of a fluid diffusion from the region enclosing the M_L 4.3 event toward the hypocenter of the M_L 5.0 earthquake, we modeled fluid flow in terms of a pore pressure perturbation caused by a point source in an isotropic fluid-saturated medium. We used the approach proposed by Noir et al. (1997) to estimate the isotropic hydraulic diffusivity (D_{iso}) by first using the hypocenter of the M_L 4.3 event as source and then the hypocenter of the M_L 5.0 as source. Figure 4b shows the r - t plots, which report the differences in time and distance between the origin time and hypocentral location of the event selected as the main event and the following events of the sequence. According to Shapiro et al. (2003), the triggering front is modeled as $r = \sqrt{4\pi Dt}$ where D is the scalar diffusivity corresponding to $D_{iso}/4$. The two plots are obtained by using 708 and 1,067 events, respectively,

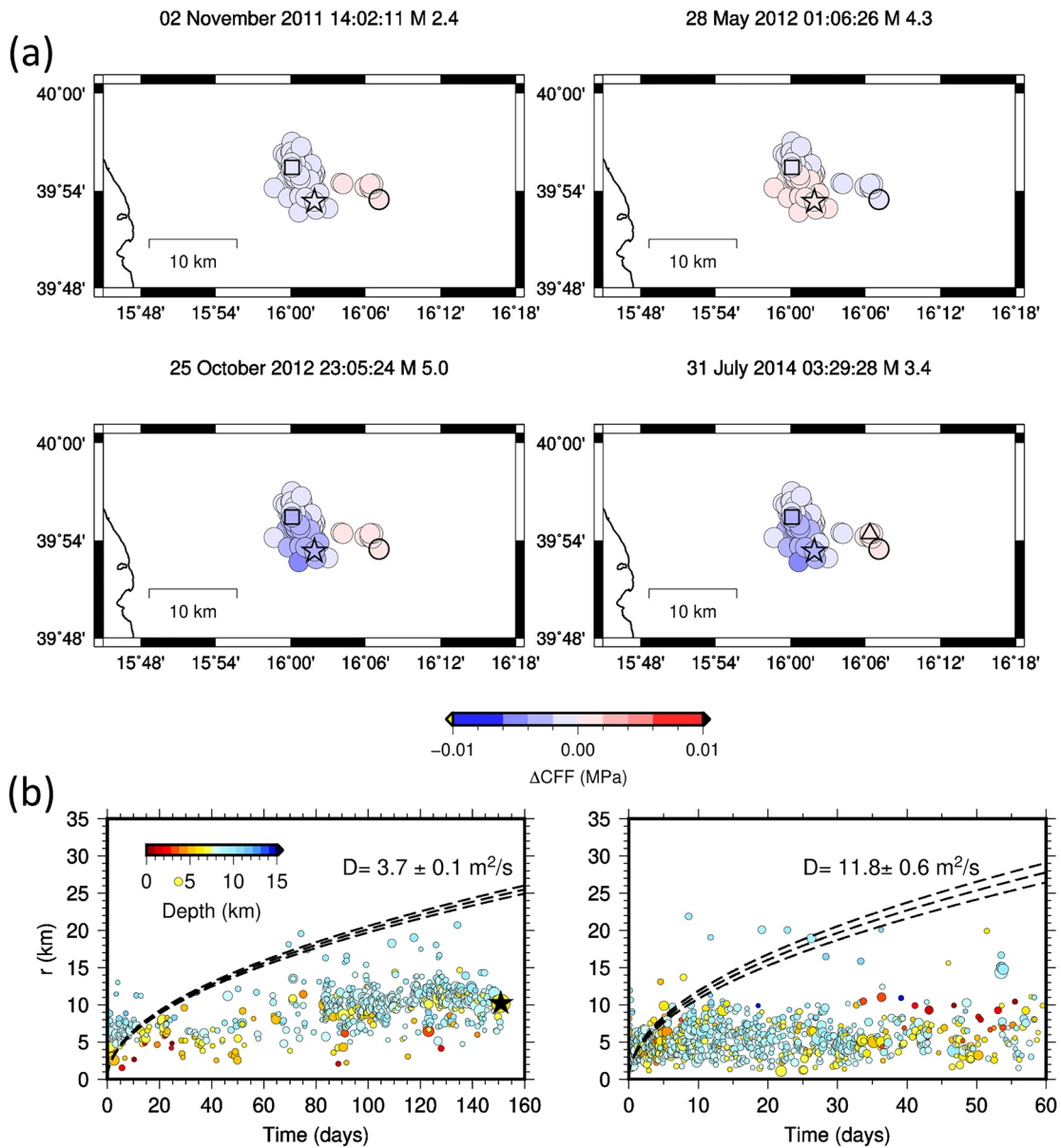


Figure 4. (a) Cumulative Coulomb stress change computed at the time of four selected earthquakes. In the panels, the locations of the M_L 4.3 (circle) and M_L 5.0 (star) events, of the first (square), and last event (triangle) of the sequence, occurred on July 31, 2014 M_L 3.4, are reported. (b) The left panel reports the results of diffusivity analysis when the M_L 4.3 event is considered as source event and all the earthquakes up to the occurrence of M_L 5.0 event (black star) are considered. The right panel reports the same analysis but considering the M_L 5.0 event as source event and the events occurring in the next 2 months. The dashed lines correspond to the inferred triggering front and to ± 1 standard deviation of the diffusivity value (D).

with magnitude larger than the minimum magnitude of completeness (M_c 1.3). The results suggest that the seismicity distribution for the first considered period was actually driven by pore-pressure diffusion with diffusivity value of $3.7 \pm 0.1 \text{ m}^2/\text{s}$. In fact, aside from the first very early days after the M_L 4.3 earthquake, all the events in the sequence lie below the triggering front. As for the second period, the results suggest that, if pore pressure diffusion occurred, it eventually took place only in the first 10–15 days after the M_L 5.0 event with a diffusivity value of $11.8 \pm 0.6 \text{ m}^2/\text{s}$.

In conclusion, our results confirm the presence of fluids in the investigated volume at pressure higher than hydrostatic value, which, together with aseismic processes, may have been the driving forces of the Pollino sequence. High pore fluid pressure explains the triggering of events also on faults non-optimally oriented with respect to the regional stress pattern. Finally, we find that the delayed triggering of the M_L 5.0 event,

which occurred about 150 days after the M_L 4.3 earthquake, seems to be compatible with a pore pressure diffusion mechanism. However, this can be confirmed by only applying more thorough analyses, which are beyond the scope of the present study.

Data Availability Statement

Focal mechanisms utilized in this study are those published in the studies by Totaro et al. (2015) and Napolitano et al. (2021). Earthquakes location and magnitude are available in the Zenodo repository <https://doi.org/10.5281/zenodo.4891146>.

Acknowledgments

This study has been supported by PRIN-2017 MATISSE Project, No 20177EPPN2, funded by the Italian Ministry of Education and Research. Figures have been generated with the Generic Mapping Tools (GMT; Wessel & Smith, 1991). Open Access Funding provided by Università degli Studi del Sannio within the CRUI-CARE Agreement.

References

- Balasco, M., Lapenna, V., Romano, G., Siniscalchi, A., Stabile, T. A., & Telesca, L. (2014). Electric and magnetic field changes observed during a Seismic Swarm in Pollino Area (Southern Italy). *Bulletin of the Seismological Society of America*, 104, 1289–1298. <https://doi.org/10.1785/0120130183>
- Barberi, G., Cosentino, M. T., Gervasi, A., Guerra, I., Neri, G., & Orecchio, B. (2004). Crustal seismic tomography in the Calabrian Arc region, south Italy. *Physics of the Earth and Planetary Interiors*, 147(4), 297–314. <https://doi.org/10.1016/j.pepi.2004.04.005>
- Bott, M. H. P. (1959). The mechanics of oblique slip faulting. *Geological Magazine*, 96(2), 109–117. <https://doi.org/10.1017/S0016756800059987>
- Brocher, T. M. (2005). Empirical relations between elastic wavespeeds and density in the Earth's crust. *Bulletin of the Seismological Society of America*, 95, 2081–2092. <https://doi.org/10.1785/0120050077>
- Brozzetti, F., Cirillo, D., de Nardis, R., Cardinali, M., Lavecchia, G., Orecchio, B., et al. (2017). Newly identified active faults in the Pollino seismic gap, southern Italy, and their seismotectonic significance. *Journal of Structural Geology*, 94, 13–31. <https://doi.org/10.1016/j.jsg.2016.10.005>
- Brozzetti, F., Lavecchia, G., Mancini, G., Milana, G., & Cardinali, M. (2009). Analysis of the 9 September 1998 Mw 5.6 Mercure earthquake sequence (southern Apennines, Italy): A multidisciplinary approach. *Tectonophysics*, 476, 210–225. <https://doi.org/10.1016/j.tecto.2008.12.007>
- Camassi, R., Castelli, V., Molin, D., Bernardini, F., Caracciolo, C. H., Ercolani, E., & Postpischl, L. (2011). Materiali per un catalogo dei terremoti italiani: Eventi sconosciuti, rivalutati o riscoperti. *Quaderni di Geofisica*, 96.
- Cheloni, D., D'Agostino, N., Selvaggi, G., Avallone, A., Fornaro, G., Giuliani, R., et al. (2017). Aseismic transient during the 2010–2014 seismic swarm: Evidence for longer recurrence of $M \geq 6.5$ earthquakes in the Pollino gap (Southern Italy)? *Scientific Reports*, 7, 576. <https://doi.org/10.1038/s41598-017-00649-z>
- Cinti, F. R., Cucci, L., Pantosti, D., D'Addezio, G., & Meghraoui, M. (1997). A major seismogenic fault in a “silent area” the Castrovillari Fault (Southern Apennines, Italy). *Geophysical Journal International*, 130, 595–605. <https://doi.org/10.1111/j.1365-246x.1997.tb01855.x>
- Convertito, V., De Matteis, R., Improta, L., & Pino, N. A. (2020). Fluid-triggered aftershocks in an anisotropic hydraulic conductivity geological complex: The case of the 2016 Amatrice Sequence, Italy. *Frontiers of Earth Science*, 8, 541323. <https://doi.org/10.3389/feart.2020.541323>
- Di Luccio, F., Ventura, G., Di Giovambattista, R., Piscini, A., & Cinti, F. R. (2010). Normal faults and thrusts reactivated by deep fluids: The 6 April 2009 Mw 6.3 L'Aquila earthquake, central Italy. *Journal of Geophysical Research*, 115, B06315. <https://doi.org/10.1029/2009jb007190>
- Doglioni, C., Barba, S., Carminati, E., & Riguzzi, F. (2014). Fault on-off versus coseismic fluids reaction. *Geoscience Frontiers*, 5, 767–780. <https://doi.org/10.1016/j.gsf.2013.08.004>
- Ferranti, L., Milano, G., & Pierro, M. (2017). Insights on the seismotectonics of the western part of northern Calabria (southern Italy) by integrated geological and geophysical data: Coexistence of shallow extensional and deep strike-slip kinematics. *Tectonophysics*, 721, 372–386. <https://doi.org/10.1016/j.tecto.2017.09.020>
- Ferranti, L., Palano, M., Cannavò, F., Mazzella, M. E., Oldow, J. S., Gueguen, E., et al. (2014). Rates of geodetic deformation across active faults in southern Italy. *Tectonophysics*, 621, 101–122. <https://doi.org/10.1016/j.tecto.2014.02.007>
- Frepoli, A., Maggi, C., Cimini, G. B., Marchetti, A., & Chiappini, M. (2011). Seismotectonic of southern Apennines from recent passive seismic experiments. *Journal of Geodynamics*, 51, 110–124. <https://doi.org/10.1016/j.jog.2010.02.007>
- King, G. C., Stein, R. S., & Lin, J. (1994). Static stress changes and the triggering of earthquakes. *Bulletin of the Seismological Society of America*, 84(3), 935–953.
- Maggi, C., Frepoli, A., Cimini, G. B., Console, R., & Chiappini, M. (2009). Recent seismicity and crustal stress field in the Lucanian Apennines and surrounding areas (Southern Italy): Seismotectonic implications. *Tectonophysics*, 463(1–4), 130–144. <https://doi.org/10.1016/j.tecto.2008.09.032>
- Malagnini, L., Lucente, F. P., De Gori, P., Akinci, A., & Munafo, I. (2012). Control of pore fluid pressure diffusion on fault failure mode: Insights from the 2009 L'Aquila seismic sequence. *Journal of Geophysical Research*, 117, B05302. <https://doi.org/10.1029/2011jb008911>
- Margheriti, L., Amato, A., Braun, T., Cecere, G., D'Ambrosio, C., De Gori, P., et al. (2013). *Emergenza nell'area del Pollino: le attività della rete sismica mobile* (Vol. 252, p. 2013). Rapporti tecnici INGV. (ISSN 2039-7941).
- Michael, A. J. (1987). Use of focal mechanisms to determine stress: A control study. *Journal of Geophysical Research*, 92, 357–368. <https://doi.org/10.1029/JB092iB01p00357>
- Michetti, A. M., Ferrelì, L., Esposito, E., Porfido, S., Blumetti, A. M., Vittori, E., et al. (2000). Ground effects during the 9 September 1998, Mw = 5.6, Lauria earthquake and the seismic potential of the “aseismic” Pollino region in southern Italy. *Seismological Research Letters*, 71(1), 31–46. <https://doi.org/10.1785/gssrl.71.1.31>
- Miller, S. A. (2020). Aftershocks are fluid-driven and decay rates controlled by permeability dynamics. *Nature Communications*, 11, 5787. <https://doi.org/10.1038/s41467-020-19590-3>
- Miller, S. A., Collettini, C., Chiaraluce, L., Cocco, M., Barchi, M., Boris, J., & Kraus, P. (2004). Aftershocks driven by a high-pressure CO₂ source at depth. *Nature*, 427, 724–727. <https://doi.org/10.1038/nature02251>
- Muir-Wood, R., & King, G. C. P. (1993). Hydrological signatures of earthquake strain. *Journal of Geophysical Research*, 98, 22035–22068. <https://doi.org/10.1029/93JB02219>

- Napolitano, F., De Siena, L., Gervasi, A., Guerra, I., Scarpa, R., & La Rocca, M. (2020). Scattering and absorption imaging of a highly fractured fluid-filled seismogenic volume in a region of slow deformation. *Geoscience Frontiers*, *11*, 989–998. <https://doi.org/10.1016/j.gsf.2019.09.014>
- Napolitano, F., Galluzzo, D., Gervasi, A., Scarpa, R., & La Rocca, M. (2021). Fault imaging at Mt. Pollino (Italy) from relative location of microearthquakes. *Geophysical Journal International*, *224*(1), 637–648. <https://doi.org/10.1093/gji/ggaa407>
- Noir, J., Jacques, E., Bekri, S., Adler, P. M., Tapponier, P., & King, G. C. P. (1997). Fluid flow triggered migration of events in the 1989 Dobi earthquake sequence of central Afar. *Geophysical Research Letters*, *24*, 2335–2338. <https://doi.org/10.1029/97gl02182>
- Palano, M., Piromallo, C., & Chiarabba, C. (2017). Surface imprint of toroidal flow at retreating slab edges: The first geodetic evidence in the Calabrian subduction system. *Geophysical Research Letters*, *44*(2), 845–853. <https://doi.org/10.1002/2016gl071452>
- Passarelli, L., Hainzl, S., Cesca, S., Maccaferri, F., Mucciarelli, M., Roessler, D., et al. (2015). Aseismic transient driving the swarm-like seismic sequence in the Pollino range, Southern Italy. *Geophysical Journal International*, *201*(3), 1553–1567. <https://doi.org/10.1093/gji/ggv111>
- Piana Agostinetti, N., & Amato, A. (2009). Moho depth and V_p/V_s ratio in peninsular Italy from teleseismic receiver functions. *Journal of Geophysical Research*, *114*(B6), B06303. <https://doi.org/10.1029/2008jb005899>
- Reasenber, P. A., & Simpson, R. W. (1992). Response of regional seismicity to the static stress change produced by the Loma Prieta earthquake. *Science*, *255*, 1687–1690. <https://doi.org/10.1126/science.255.5052.1687>
- Serpelloni, E., Anzidei, M., Baldi, P., Casula, G., & Galvani, A. (2005). Crustal velocity and strain-rate fields in Italy and surrounding regions: New results from the analysis of permanent and non-permanent GPS networks. *Geophysical Journal International*, *161*(3), 861–880. <https://doi.org/10.1111/j.1365-246X.2005.02618.x>
- Shapiro, S., Patzig, R., Rothert, E., & Rindschwentner, J. (2003). Triggering of seismicity by pore-pressure perturbations: Permeability-related signatures of the phenomenon. *Pure and Applied Geophysics*, *160*, 1051–1066. <https://doi.org/10.1007/PL00012560>
- Sketsiou, P., De Siena, L., Gabrielli, S., & Napolitano, F. (2021). 3-D attenuation image of fluid storage and tectonic interactions across the Pollino fault network. *Geophysical Journal International*, *226*(1), 536–547. <https://doi.org/10.1093/gji/ggab109>
- Sketsiou, P., Napolitano, F., Zenonos, A., & De Siena, L. (2020). New insights into seismic absorption imaging. *Physics of the Earth and Planetary Interiors*, *298*, 106337. <https://doi.org/10.1016/j.pepi.2019.106337>
- Terakawa, T., Miller, S. A., & Deichmann, N. (2012). High fluid pressure and triggered earthquakes in the enhanced geothermal system in Basel, Switzerland. *Journal of Geophysical Research*, *117*, B07305. <https://doi.org/10.1029/2011JB008980>
- Terakawa, T., Zoporowski, A., Galvan, B., & Miller, S. A. (2010). High-pressure fluid at hypocentral depths in the L'Aquila region inferred from earthquake focal mechanisms. *Geology*, *38*(11), 995–998. <https://doi.org/10.1130/g31457.1>
- Tertulliani, A., & Cucci, L. (2014). New insights on the strongest historical earthquake in the Pollino region (southern Italy). *Seismological Research Letters*, *85*, 743–751. <https://doi.org/10.1785/0220130217>
- Totaro, C., Koukakov, I., Orecchio, B., & Presti, D. (2014). Detailed crustal structure in the area of the southern Apennines–Calabrian Arc border from local earthquake tomography. *Journal of Geodynamics*, *82*, 87–97. <https://doi.org/10.1016/j.jog.2014.07.004>
- Totaro, C., Orecchio, B., Presti, D., Scolaro, S., & Neri, G. (2016). Seismogenic stress field estimation in the Calabrian Arc region (south Italy) from a Bayesian approach. *Geophysical Research Letters*, *43*, 8960–8969. <https://doi.org/10.1002/2016gl070107>
- Totaro, C., Presti, D., Billi, A., Gervasi, A., Orecchio, B., Guerra, I., & Neri, G. (2013). The ongoing seismic sequence at the Pollino Mountains, Italy. *Seismological Research Letters*, *84*(6), 955–962. <https://doi.org/10.1785/0220120194>
- Totaro, C., Seeber, L., Waldhauser, F., Steckler, M., Gervasi, A., Guerra, I., et al. (2015). An intense earthquake swarm in the southernmost Apennines: Fault architecture from high-resolution hypocenters and focal mechanisms. *Bulletin of the Seismological Society of America*, *105*(6), 3121–3128. <https://doi.org/10.1785/0120150074>
- Tung, S., & Masterlark, T. (2018). Delayed poroelastic triggering of the 2016 October Visso earthquake by the August Amatrice earthquake, Italy. *Geophysical Research Letters*, *45*, 2221–2229. <https://doi.org/10.1002/2017GL076453>
- Valensise, G., & Guidoboni, E. (2000). Towards new research strategies: Silent seismogenic areas or silent sources? *Annali di Geofisica*, *43*, 16403. <https://doi.org/10.1038/s41598-017-14550-2>
- Valerio, E., Tizzani, P., Carminati, E., & Doglioni, C. (2017). Longer aftershocks duration in extensional tectonic settings. *Scientific Reports*, *7*, 16403. <https://doi.org/10.1038/s41598-017-14550-2>
- Vavrycuk, V. (2014). Iterative joint inversion for stress and fault orientations from focal mechanisms. *Geophysical Journal International*, *199*, 69–77. <https://doi.org/10.1093/gji/ggu224>
- Wallace, R. E. (1951). Geometry of shearing stress and relation of faulting. *The Journal of Geology*, *59*(2), 118–130. <https://doi.org/10.1086/625831>
- Wang, R., Lorenzo Martin, F., & Roth, F. (2006). PSGRN/PSCMP – A new code for calculating co- and post-seismic deformation, geoid and gravity changes based on the viscoelastic-gravitational dislocation theory. *Computers & Geosciences*, *32*(4), 527–541. <https://doi.org/10.1016/j.cageo.2005.08.006>
- Wells, D. L., & Coppersmith, K. J. (1994). New empirical relationships among magnitude, rupture length, rupture width, rupture area, and surface displacement. *Bulletin of the Seismological Society of America*, *84*(4), 974–1002.
- Wessel, P., & Smith, W. H. F. (1991). Free software helps map and display data. *Eos, Transactions, American Geophysical Union*, *72*(41), 441–446. <https://doi.org/10.1029/90eo00319>
- Wiemer, S., & Wyss, M. (2000). Minimum magnitude of completeness in earthquake catalogs: Examples from Alaska, the Western United States, and Japan. *Bulletin of the Seismological Society of America*, *90*(4), 859–869. <https://doi.org/10.1785/0119990114>
- Yabuki, T., & Matsu'ura, M. (1992). Geodetic data inversion using a Bayesian information criterion for spatial distribution of fault slip. *Geophysical Journal International*, *109*(2), 363–375. <https://doi.org/10.1111/j.1365-246X.1992.tb00102.x>
- Zoback, M. D. (2010). *Reservoir geomechanics*. Cambridge University Press.